Int. J. Solids Structures Vol. 23, No. 7, pp. 937–946, 1987
Printed in Great Britain.

0020-7683/87 $3.00+ .00
Pergamon Journals Ltd.

THE EFFECTS OF LAMB WAVES ON THE SONAR CROSS-SECTIONS OF ELASTIC SPHERICAL SHELLS

V. M. AYRES, G. C. GAUNAURD and C. Y. TSUI
Naval Surface Weapons Center, White Oak Lab, 10901 New Hampshire Avenue, Silver Spring, MD 20903-5000, U.S.A.

and

M. F. WERBY
Naval Ocean R&D Activity, Code 221, NSTL Station, MI 39529, U.S.A.

(*Received* 31 *March* 1986; *in revised form* 28 *August* 1986)

Abstract—We study the interaction of a plane sound wave with a fixed, elastic, tungsten carbide (WC), spherical shell in water. The shell is air filled and its motions are described by the exact three-dimensional equations of elastodynamics. The form-function of the problem is obtained by solving the resulting classical boundary value problem for the required coefficients. The form-function so obtained is displayed vs non-dimensional frequency k_1a in a very wide spectral band never obtained before in the analysis of this type of problem. Various physical effects are presented as the causes of the several features influencing the shape of the form-function in various spectral regimes. The computed plots serve to corroborate these interpretations, and to quantitatively exhibit these effects for both thin and thick shells. We find that Lamb waves of various orders combined with waves undergoing multiple bounces inside the shell thickness, and with externally diffracted Franz waves, serve to explain all the mechanisms of scattering and the resonance features displayed in the cross-sectional plots at all frequencies. Lamb waves of order zero and one are dominant over all other mechanisms observable within this wide spectral band. The influences of specular reflections and Franz-wave diffraction contributions are shown to be minimal.

1. INTRODUCTION

Modern studies of sound scattering by elastic, air-filled, shells in water started in the 1960s. The spherical shell in particular was first treated by Goodman and Stern[1], and afterwards, by Hickling and co-workers[2–4]. These papers described the shell motions by the exact equations of three-dimensional elasticity. Other treatments of the problem in subsequent works[5–8], used shell theories as well. Details of the elasticity formulation required to set up and solve such boundary value problems for separable geometries have been available for some time, and have been summarized in convenient uniform and systematic forms[9]. The specific case of the *spherical* shell coated with a viscoelastic absorbing layer showed how the shell's backscattering cross-section and the resonance features contained within it, could be modified by means of the absorbing layer[10]. The theoretical analysis of the sound/structure interaction problem that occurs when a plane wave falls on a submerged spherical shell has been studied by means of the resonance scattering theory (RST) [10]. The methodology of the RST has been presented in a series of papers[10–17], and will not be re-examined here. However, we will use its general principles founded on background subtraction and resonance isolation[17] to interpret the high-frequency response of both thin and thick shells undergoing resonance scattering. This interpretation can be made in terms of symmetric and antisymmetric Lamb waves[18] as well as by a combination of waves undergoing multiple bounces inside the shell thickness added to contributions from diffracted Franz waves[19–21] in the water, or to strong specular reflections. In what follows, we will obtain and display the form-function of a spherical shell governed by the exact elasticity equations, up to very high frequencies (namely, $k_1a = 200$). Modern computational advances permit these computations for bodies as complex as shells governed by the exact three-dimensional elastodynamic equations. Until recently, these high spectral regions could only be reached by means of (qualitative) asymptotic methods such as the Watson–Sommerfeld method[19–21]. The present availability of exact, quantitative, computed results, verifies the physical interpretations and the spectral influence of the

various effects that we present in this work. In particular, we analyze the effects of the first few Lamb wave modes on the cross-section of the shell, which become very evident at the higher frequencies that we display here. These Lamb wave modes are dominant over the other three possible contributions. Although not examined here, the conclusions that have emerged from this analysis remain valid when the shell is insonified by finite sound beams of pulses, in the manner briefly studied in some earlier works[22].

2. THEORETICAL BACKGROUND

A plane wave is incident on an elastic, air-filled, spherical shell in water. The total pressure field in the water is

$$p_1(r,\theta,t) = p_0\, e^{-i\omega t} \sum_{n=0}^{\infty} i^n(2n+1)P_n(\cos\theta)\,[j_n(k_1 r)+A_n h_n^{(1)}(k_1 r)]. \tag{1}$$

The elastic (Debye) potentials within the shell are

$$\begin{aligned}\phi_{d_2} &= p_0\, e^{-i\omega t} \sum_{n=0}^{\infty} i^n(2n+1)P_n(\cos\theta)\,[B_n j_n(k_{d_2} r)+C_n y_n(k_{d_2} r)]\\ \psi_{s_2} &= p_0\, e^{-i\omega t} \sum_{n=0}^{\infty} i^n(2n+1)P_n(\cos\theta)\,[D_n j_n(k_{s_2} r)+E_n y_n(k_{s_2} r)].\end{aligned} \tag{2}$$

The pressure field inside the shell is

$$p_3 = p_0\, e^{-i\omega t} \sum_{n=0}^{\infty} i^n(2n+1)P_n(\cos\theta)F_n j_n(k_3 r). \tag{3}$$

The various wave numbers in the three media are

$$k_1 = \frac{\omega}{c_1}; \qquad k_{d_2} = \frac{\omega}{c_{d_2}}, \quad k_{s_2} = \frac{\omega}{c_{s_2}}; \qquad k_3 = \frac{\omega}{c_3} \tag{4}$$

where c_1 and c_3 are the sound speeds in water and the air, respectively, and c_{d_2}, c_{s_2} are the dilatational and shear wave speeds in the shell. Water is medium 1, the shell is medium 2, and air is medium 3. The six sets of constants A_n, B_n, C_n, D_n, E_n and F_n are determined from the boundary conditions, which are in this case

$$\begin{aligned}&\tau_{rr}^{(2)} = -p_1; \qquad u_r^{(1)} = u_r^{(2)}; \quad \text{and} \quad \tau_{r\theta}^{(2)} = 0 \quad \text{at} \quad r = a\\ &\tau_{rr}^{(2)} = -p_3; \qquad u_r^{(2)} = u_r^{(3)}; \quad \text{and} \quad \tau_{r\theta}^{(2)} = 0 \quad \text{at} \quad r = b\end{aligned} \tag{5}$$

where a and b are the outer and inner radius of the spherical shell. Expressions for the stresses and displacements in terms of the Debye potentials in the shell or the two fluids have been determined in earlier work[9–12] in spherical (and other) coordinate systems. Use of these expressions in the solutions (i.e. eqns (1)–(4)) and in the boundary conditions (eqn (5)) yields the following algebraic system of equations:

$$\mathscr{D}[x] = \begin{bmatrix} d_{11} & d_{12} & d_{13} & d_{14} & d_{15} & 0 \\ d_{21} & d_{22} & d_{23} & d_{24} & d_{25} & 0 \\ 0 & d_{32} & d_{33} & d_{34} & d_{35} & 0 \\ 0 & d_{42} & d_{43} & d_{44} & d_{45} & d_{46} \\ 0 & d_{52} & d_{53} & d_{54} & d_{55} & d_{56} \\ 0 & d_{62} & d_{63} & d_{64} & d_{65} & 0 \end{bmatrix} \begin{bmatrix} A_n \\ B_n \\ C_n \\ D_n \\ E_n \\ F_n \end{bmatrix} = \begin{bmatrix} A_1^* \\ A_2^* \\ 0 \\ 0 \\ 0 \\ 0 \end{bmatrix} = [b] \tag{6}$$

which can be solved by Cramer's rule for any of the sets of coefficients $A_n, B_n, \ldots$. The elements of matrix $\mathscr{D}$ and column vector $[b]$ are found by application of the boundary conditions and are all listed in the Appendix, in non-dimensional form.

The backscattering cross-section, σ, is given by

$$\frac{\sigma}{\pi a^2} = \left| \frac{2}{ik_1 a} \sum_{n=0}^{\infty} (-1)^n A_n (2n+1) \right|^2 = |f_\infty(\pi)|^2 \tag{7}$$

which is normalized to πa^2, and where A_n is the only one of the six sets of coefficients that could enter its expression. The form-function $|f_\infty(\pi)|$ is usually the quantity computed or measured.

This form-function contains the partial waves $f_n(\pi)$ (also referred to as normal modes, or the terms of the Rayleigh series) as follows:

$$|f_\infty(\pi)| = \left| \sum_{n=0}^{\infty} f_n(\pi) \right| = \left| \frac{1}{ik_1 a} \sum_{n=0}^{\infty} (-1)^n (2n+1)(S_n - 1) \right| \tag{8}$$

where we have used the 'Optical Theorem': $2A_n = S_n - 1$, where S_n is the scattering function of the problem.

The coefficients $2A_n$ in eqn (8), are the ratios of two 6×6 determinants, which according to Cramer's rule are as follows:

$$2A_n = \frac{2}{|D_n|} \begin{vmatrix} A_1^* & d_{12} & d_{13} & d_{14} & d_{15} & 0 \\ A_2^* & d_{22} & d_{23} & d_{24} & d_{25} & 0 \\ 0 & d_{32} & d_{33} & d_{34} & d_{35} & 0 \\ 0 & d_{42} & d_{43} & d_{44} & d_{45} & d_{46} \\ 0 & d_{52} & d_{53} & d_{54} & d_{55} & d_{56} \\ 0 & d_{62} & d_{63} & d_{64} & d_{65} & d_{66} \end{vmatrix} = S_n - 1 \tag{9}$$

where $|D_n|$ is the determinant of matrix $\mathscr{D}$ in eqn (6). The coefficients A_n, with the special normalized form of the d_{ij} elements in the Appendix, make these spherical shell results compatible and consistent with earlier work[13–16] on this subject. Figure 1 shows the geometry of the problem.

3. PHYSICAL INTERPRETATION OF THE FORM-FUNCTION

The pertinent material properties of WC are as follows. The density is $\rho_2 = 13.1$ g cm^{-3}, the speed of dilatational waves is $c_{d_2} = 6.95 \times 10^5$ cm s^{-1}, and the speed of shear waves is $c_{s_2} = 3.94 \times 10^5$ cm s^{-1}. Those of water and air were given earlier[10–12].

Using a CDC CYBER 170/720 computer we have implemented the normal-mode, exact, elasticity formulation for the form-function given in eqns (8) and (9). Computer codes to perform similar calculations[9] have been available at NSWC since 1975. We can generate the form-function for any material composition combination for shell, filler, and outer fluid, of any thickness, in any frequency band of interest. The only limitation at

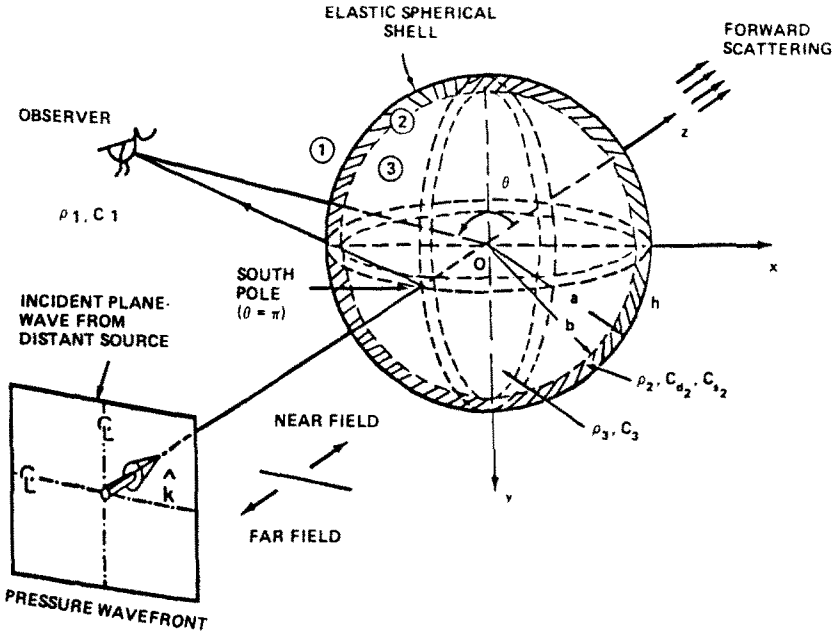

Fig. 1. Shell geometry and incident plane wave.

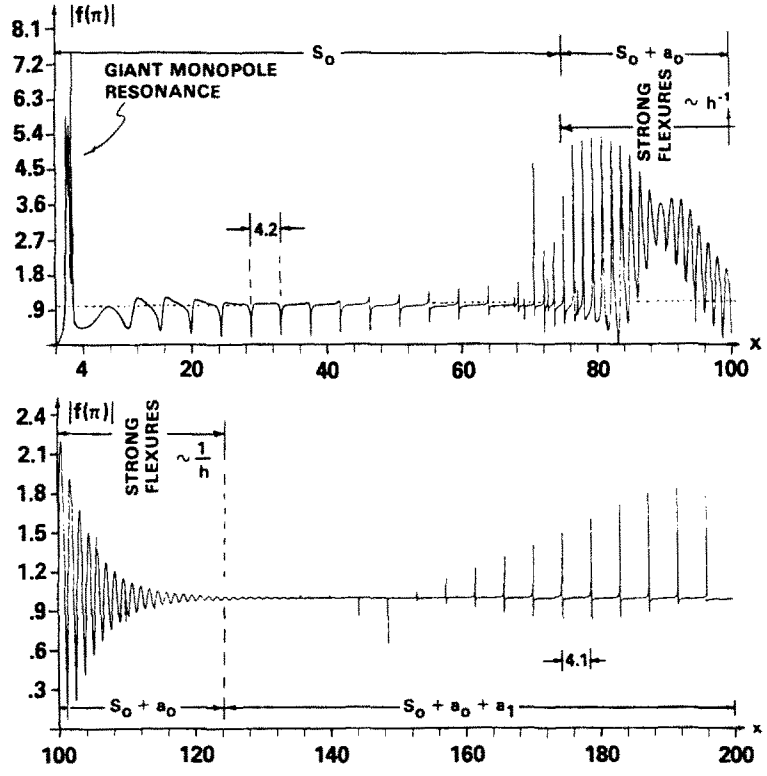

Fig. 2. (a) Form-function of a thin WC, air-filled, spherical shell of thickness $h = 1\%$ in water, in the range: $0 \leqslant x \leqslant 100$. (b) Same, in the range: $100 \leqslant x \leqslant 200$. Ordinates are expanded for clarity.

present seems to be the cost of the run. All the form-function results to be displayed here are for an air-filled, WC, spherical shell in water, in the extremely wide spectral band: $0 \leqslant k_1 a \leqslant 200$. We will show two different thicknesses to illustrate what we consider "thick" and "thin" behaviors.

Figure 2 shows the form-function of an air-filled, WC, spherical shell of relative thickness $h = 1 - b/a = 0.01 = 1\%$ in water, vs non-dimensional frequency $x_1 \equiv k_1 a$. This

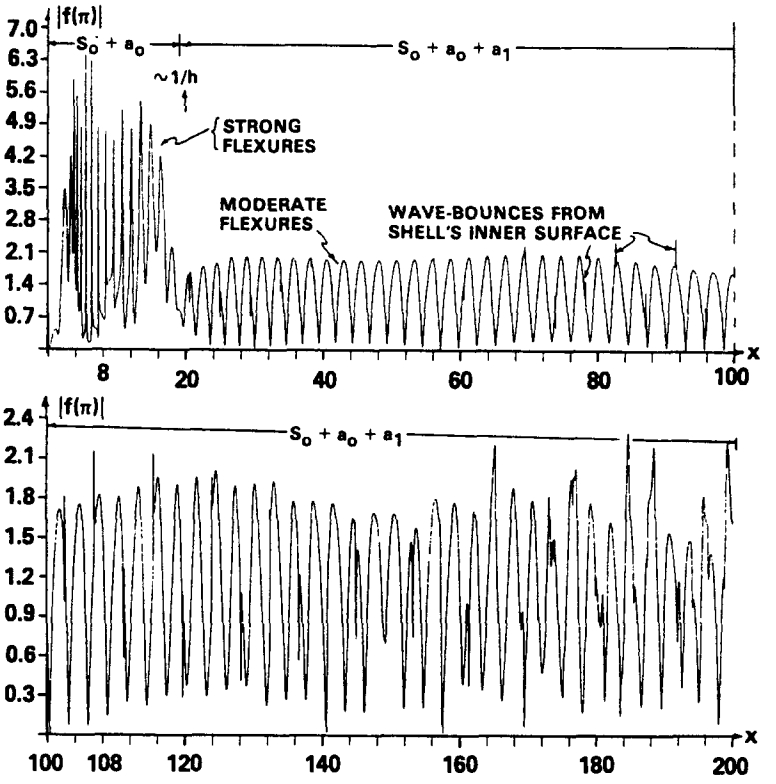

Fig. 3. (a) Form-function of a thick WC, air-filled, spherical shell of thickness $h = 5\%$ in water, in the range: $0 \leqslant x \leqslant 100$. (b) Same, in the range: $100 \leqslant x \leqslant 200$. Ordinates are expanded for clarity.

could be considered to be the spectral response of a thin shell. Although the thickness is quite small, the "proper" background that isolates the resonances is still the rigid one. Figure 2(a) shows the band $0 \leqslant k_1 a \leqslant 100$, and Fig. 2(b) displays the band: $100 \leqslant k_1 a \leqslant 200$.

Based on earlier work[17] that need not be repeated here, we now know that the *rigid* background is the "proper background" we must choose to isolate most shell's resonance features in their form-function. It was shown[17] that the rigid background isolates shell resonances for all thicknesses down to very thin values of h such as 10^{-3}. Below this value, one must use the soft background to isolate resonances. In the present work we remain above the value $h = 10^{-2} = 1\%$, therefore, the rigid background is always suitable to isolate resonances. More detailed studies will be further pursued elsewhere.

Figures 3(a) and (b) repeat the same displays, in the same bands, for a WC shell of relative thickness $h = 5\%$. This could be considered the spectral response of a thick shell, but obtained exactly from the three-dimensional equations of dynamic elasticity as described above, since no shell theory approximation was used here. Shells for which $h > 5\%$ are rare in practical cases for which this analysis could be applicable.

The background suppression process described above is basic to the RST because this is how the resonance spectrogram[11] of macroscopic targets can be isolated and extracted from its returned echoes. The physical interpretation introduced by the RST is best seen by rewriting the $(S_n - 1)$ factor in eqn (8) in the form[10, 14, 15]

$$S_n - 1 = 2\mathrm{i}\, \mathrm{e}^{2\mathrm{i}\xi_n^{(r)}} \left[\sum_{j=1}^{N} \frac{-\Gamma_{nj}^{(r)}/2}{x - x_{nj}^{(r)} + \mathrm{i}(\Gamma_{nj}^{(r)}/2)} + \mathrm{e}^{-\mathrm{i}\xi_n^{(r)}} \sin \xi_n^{(r)} \right] \tag{10}$$

which explicitly exhibits the resonance/background interaction always present within each partial wave. It is possible to express this interaction in *analytic* form, since in this case the body is separable. Resonance and background contributions are respectively represented by the two terms being added inside the bracket. The definitions of $x_{nj}^{(r)}$, $\Gamma_{nj}^{(r)}$ ... have been given earlier[10–13] in related cases pertaining to other combinations of materials and

geometries. We should repeat that in the case of an extremely thin shell, $h \leqslant 0.1\%$, the resonances will be isolated by subtraction of the *soft* background. This is so because in this case the shell wall becomes tenuous, and the shell takes on more of the character of a gas bubble in a liquid.

The spectral shape of the form-function is affected by contributions due to the scatterer's shape and/or to the penetrable composition. Body *shape* effects are:

(a) specular reflections from the shell's outer surface $r = a$,
(b) diffracted Franz-type waves circumnavigating the shell.

Specular reflections produce *no* extrema in the form-function. Franz waves are analogous to those around rigid bodies, and can only cause *minor* extrema in the form-function. Both these effects are small, and play minor roles.

Contributions due to the shell's *penetrability* are basically of two types:

(a) Waves scattered from the shell's inner surface $r = b$. These waves can bounce many times inside the thickness. For *thin* shells they are more manifest at high k_1a. For *thick* shells they are more important at low k_1a.

(b) Symmetric and antisymmetric Lamb waves[18] of order zero (i.e. s_0 and a_0, respectively). For thin shells, s_0 is dominant. The a_0-wave manifests itself only in the region of "strong flexures", where $x_1h \approx 1$. Higher-order Lamb waves are important only at very high k_1a. It follows that a thick shell has a form-function almost totally dominated by the "momentless" and "flexural" Lamb waves, s_0 and a_0, within the band $0 \leqslant k_1a \leqslant 200$.

The influence of each of the effects described above may be determined from an analysis of the plots displayed in Figs 2 and 3. We begin with the analysis of the behavior of a thin shell (Fig. 2). In Fig. 2(a) we see no contribution due to body shape except for the low k_1a region $0 \leqslant k_1a \leqslant 3$, in which the shell's giant monopole resonance is observed. This resonance is caused by the $n = 0$ mode. After $k_1a = 3$, a periodic pattern of "inverted U's" develops immediately. This is the effect of the Lamb mode s_0. This behavior persists until $k_1a \approx 70$, where the effect of a_0 starts to be felt. This is the region of "strong flexures" where $k_1a \equiv x_1 = h^{-1} \approx 100$. This region continues up to $x_1 \equiv k_1a \approx 120$, after which it dies out. At $k_1a \approx 160$, a new set of resonance extrema develops. This is the effect of the antisymmetric Lamb mode a_1, that goes on beyond $k_1a = 200$, where the plot ends.

We can determine the phase (or group) velocities of these waves from the periodic spacings in-between resonances in the regions $3 \leqslant k_1a \leqslant 70$, and $160 \leqslant k_1a \leqslant 200$. These waves propagate almost without dispersion (as is evidenced by the fact that the resonance spacings are quasi-uniform in both regions) and therefore $c_0^{gr} = c_0^{ph} = c_1^{gr} = c_1^{ph} = 4.15 \times 10^5$ cm s^{-1}, as we can read from Fig. 2.

The shell of Fig. 3 is a thick shell with $h = 5\% = 1/20$. There is hardly any activity due to the Lamb symmetric mode s_0, and the region of strong flexures develops immediately up to $x \equiv k_1a = h^{-1} \simeq 20$. This is followed by the moderate flexures seen in the rest of the plot (i.e. $25 \leqslant k_1a \leqslant 100$, and $100 \leqslant k_1a \leqslant 200$). The strong flexures are caused by a_0 and the moderate flexures by a_1. Higher-order Lamb modes ($l > 1$) would influence the form-function only at very high frequencies beyond $k_1a = 200$. At these high frequencies and beyond, it would be more advantageous (and less expensive) to generate these plots by means of asymptotic techniques such as the Watson–Sommerfeld method[19]. Superimposed on the a_1-effect we see additional narrow resonances; these are caused by successive wave bounces from the shell's inner surface, $r = b$.

The spacings between extrema in the region of strong flexures or in the region of moderate flexures can be used to determine the phase or the group velocities of the a_0 and a_1 waves, which are again seen to propagate almost without dispersion. This results in a value for $c_0^{gr} = c_0^{ph} = c_1^{gr} = c_1^{ph} \cong 3.1 \times 10^5$ cm s^{-1} (Fig. 3).

The entire approach shown here is exact since it is based on the general equations of dynamic elasticity, no approximation based on a shell theory having been introduced. The solution is exact because the geometry is separable and the classical normal-mode solution

is possible. For shells in water, this only happens in the spherical, cylindrical or Cartesian coordinate systems.

We conclude with some remarks about the phase velocities of the first two (s_0, s_1) and antisymmetric (a_0, a_1) Lamb waves for a WC plate in vacuum. Many authors have studied these waves, and expressions for their phase velocities are known to be given[18] by the roots of the following equations.

For the symmetric branches $(s_j, j = 0, 1, \ldots)$

$$\frac{\tan\left[k_s d\sqrt{\left(1-\frac{c_s^2}{c^2}\right)}\right]}{\tan\left[k_s d\sqrt{\left(\frac{c_s^2}{c_d^2}-\frac{c_s^2}{c^2}\right)}\right]} = -\frac{4\frac{c_s^2}{c^2}\sqrt{\left(1-\frac{c_s^2}{c^2}\right)}\sqrt{\left(\frac{c_s^2}{c_d^2}-\frac{c_s^2}{c^2}\right)}}{\left(2\frac{c_s^2}{c^2}-1\right)^2}. \tag{11}$$

For the antisymmetric branches $(a_j, j = 0, 1, \ldots)$

$$\frac{\tan\left[k_s d\sqrt{\left(1-\frac{c_s^2}{C^2}\right)}\right]}{\tan\left[k_s d\sqrt{\left(\frac{c_s^2}{c_d^2}-\frac{c_s^2}{c^2}\right)}\right]} = -\frac{\left(2\frac{c_s^2}{C^2}-1\right)^2}{4\frac{c_s^2}{c^2}\sqrt{\left(1-\frac{c_s^2}{c^2}\right)}\sqrt{\left(\frac{c_s^2}{c_d^2}-\frac{c_s^2}{c^2}\right)}}. \tag{12}$$

These equations are solved for the various values of c/c_s along each branch, and are plotted vs the frequency–thickness product fd, where $2d$ is the thickness of the plate, for various values of the ratio c_d/c_s. For a metal, this ratio is a function of the Poisson ratio ν as follows:

$$\frac{c_d}{c_s} = \sqrt{\left(\frac{2-2\nu}{1-2\nu}\right)}. \tag{13}$$

For WC, the Poisson ratio is $\nu = 0.2632$, thus, the above ratio is 1.7639. Plots of the phase velocities (c/c_s) normalized to c_s, vs fd, for $c_d/c_s = 1.7639$ are shown in Fig. 4, for the first couple of symmetric and antisymmetric branches (namely, $j = 0$ and 1). In order to relate the frequency at which a certain mode in Fig. 4 affects the form-function plots shown in Figs 2 and 3, we use the following relation:

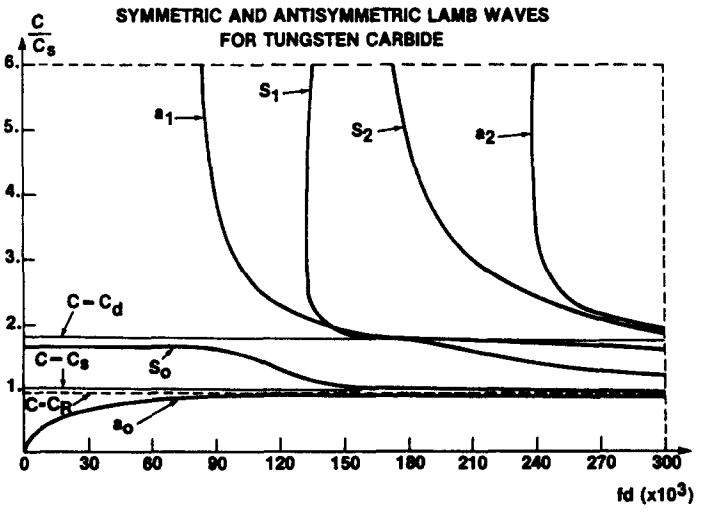

Fig. 4. Dispersion plots for the phase velocities of the first few (s_0, s_1, a_0, a_1) Lamb modes of a WC plate in water.

$$fh' = x_1 \frac{c_1}{2\pi}\left(1 - \frac{b}{a}\right) \tag{14}$$

where $h' = a - b = 2d$, which can be derived immediately on geometrical considerations. This relates the abscissas of Fig. 4 with those of Figs 2 and 3 even though Fig. 4 pertains to a flat plate and Figs 2 and 3 to a spherical shell.

We remark in closing that the dispersion curves for a free-free WC plate shown in Fig. 4 are undistinguishable from those of a fluid-loaded plate, particularly when these fluids are water and air. Tungsten carbide is one of the toughest and most rigid metals known. In view of these desirable properties, most underwater acoustic calibrating targets, particularly shells and ball bearings, are made of this substance. Although dispersion plots similar to those shown in Fig. 4 have been computed for other metals, mainly for steel[18], we have recomputed them here for WC in view of its particular usefulness for our study. We repeat that the dispersion curves in Fig. 4 for a *plate* can be used for the purpose of identifying which Lamb modes affect which portions of the backscattering cross-sections of these spherical *shells* displayed in Figs 2 and 3, provided that we use eqn (14) to relate the abscissas in Figs 2 and 3, to those of Fig. 4. This seems to be sufficient to account for the curvature correction in this type of display. The fluid-loading correction is negligible. If exact dispersion curves for the Lamb waves circumnavigating a spherical shell, fluid-loaded externally by water and internally by air, were to be rigorously computed, one would have to plot the families of roots of the determinant of matrix $\mathscr{D}$ in eqn (6) vs x_1. This calculation is not required for our present purposes and will be pursued elsewhere.

4. CONCLUSIONS

We have obtained the form-function $|f(\pi)|$ of thin and thick spherical WC shells in water, up to very high frequencies (i.e. $k_1 a = 200$). We demonstrated the influence of four effects on the frequency dependence of $f(\pi)$ and concluded that the strongest and most dominant of these effects are the Lamb symmetric and antisymmetric modes. We quantitatively exhibit the effect of each one of these modes on the form-function plots. As the frequency increases, higher and higher modes make their influence felt in the cross-sectional plots. These influences vary with shell thickness, as shown by the different spectral responses exhibited in Figs 2(a), (b) and 3(a), (b). The dispersion plots for the phase velocities of the first few Lamb modes (s_0, s_1, a_0, a_1) are obtained for WC, and the frequencies in these plots and those in Figs 2 and 3 are found to be related by a simple expression, namely eqn (14).

The non-dimensionalization *procedure* followed to obtain the above form of these elements was discussed in Ref. [21]. The above list has certain similarities with the analogous list of coefficients for a cylindrical shell given in the Appendix of Ref. [11].

Acknowledgements—The authors thank their respective Center's IR-Boards, as well as that of the Space Warfare Command (NAVSPAWARS) for their support.

REFERENCES

1. R. Goodman and R. Stern, Reflection and transmission of sound by an elastic spherical shell. *J. Acoust. Soc. Am.* **34**, 338–344 (1962).
2. R. Hickling, Analysis of echoes from a hollow metallic sphere in water. *J. Acoust. Soc. Am.* **36**, 1124–1137 (1964).
3. K. J. Diereks and R. Hickling, Echoes from hollow aluminum spheres in water. *J. Acoust. Soc. Am.* **41**, 380–393 (1967).
4. R. Hickling and R. W. Means, Scattering of FM-pulses by spherical elastic shells in water. *J. Acoust. Soc. Am.* **44**, 1246–1252 (1968).
5. A. H. Shah, C. V. Ramakrishnan and S. K. Datta, Three-dimensional and shell theory analysis of elastic waves in a hollow sphere. *J. Appl. Mech.* **36**, 431–444 (1969).
6. S. C. Tang and D. H. Y. Yen, Interaction of a plane acoustic wave with an elastic spherical shell. *J. Acoust. Soc. Am.* **47**, 1325–1333 (1970).
7. M. C. Junger and D. Feit, *Sound, Structures and their Interaction* (Art 12.6). MIT Press, Cambridge, Massachusetts (1972).

8. W. C. Fender, Scattering from an elastic spherical shell. Naval Undersea Center Technical Report NUC-TR-313, San Diego, California (October 1972).
9. G. C. Gaunaurd, Methods for solving the viscoclasticity equations for cylinder and sphere problems. Tech. Report NSWC/WO TR-76-20, 28 pp. Uncl. (ADA-025-302; March 1976).
10. G. Gaunaurd and A. Kalnins, Resonances in the sonar cross-sections of (coated) spherical shells. *Int. J. Solids Structures* **18**, 1083–1102 (1982).
11. G. Gaunaurd and D. Brill, Acoustic spectrogram and complex-frequency poles of a resonantly excited elastic tube. *J. Acoust. Soc. Am.* **75**, 1680–1693 (1984).
12. G. Gaunaurd and H. Überall, RST analysis of monostatic and bistatic acoustic echoes from an elastic sphere. *J. Acoust. Soc. Am.* **73**, 1–12 (1983).
13. L. Flax, G. Gaunaurd and H. Überall, The theory of resonance scattering. In *Physical Acoustics XV* (Edited by W. P. Mason and R. N. Thurston), Chap. 3, pp. 191–294. Academic Press, New York (1981).
14. V. M. Ayres and G. Gaunaurd, Acoustic resonance scattering by absorbing bodies, **81**, 301–311 (1987).
15. G. Gaunaurd, E. Tanglis, D. Brill and H. Ueberall, Interior and exterior resonances in acoustic scattering. Pt. I. Spherical targets, *Nuovo Cimento* **76B**, 153–175 (1983).
16. G. Gaunaurd *et al.*, Inverse scattering and the resonances of viscoelastic and electromagnetic waves. In *Wave Propagation in Viscoelastic Media*, Research Notes in Mathematics No. 52, pp. 235–257. Pitman, New York (1982).
17. G. Gaunaurd and M. Werby, Proper background choice in resonance scattering by elastic shells. *Int. J. Solids Structures* **22**, 1149–1159 (1986).
18. I. A. Viktorov, *Raleigh and Lamb Waves*, pp. 67–83. Plenum, New York (1967).
19. H. M. Nussenzveig, High-frequency scattering by a transparent sphere... *J. Math. Phys.* **10**, 82–176 (1969).
20. W. Franz, *Theory of Diffraction of Electromagnetic Waves*. Springer, Berlin (1957), in German. English Translation by NISC, Transl. 3675 of 28 Nov. (1975).
21. G. C. Gaunaurd, High-frequency acoustic scattering from submerged cylindrical shells coated with viscoelastic absorbing layers. *J. Acoust. Soc. Am.* **62**, 503–512 (1977).
22. O. P. Piddubryak and V. V. Porokhovs'kyy, Interaction between a sound beam and a hollow sphere in an acoustic fluid. *Dopov. Akad. Nauk URSR* No. 4, Series A, 49–51 (1980), in Russian.

APPENDIX

The 30 non-vanishing elements appearing in eqn (6) are as follows:

$$d_{11} = \left(\frac{\rho_1}{\rho_2}\right) k_{s_2}^2 a^2 h_n^{(1)}(k_1 a)$$

$$d_{12} = [2n(n+1) - k_{s_2}^2 a^2] j_n(k_{d_2} a) - 4k_{d_2} a j_n'(k_{d_2} a)$$

$$d_{13} = [2n(n+1) - k_{s_2}^2 a^2] y_n(k_{d_2} a) - 4k_{d_2} a y_n'(k_{d_2} a)$$

$$d_{14} = 2n(n+1)[k_{s_2} a j_n'(k_{s_2} a) - j_n(k_{s_2} a)]$$

$$d_{15} = 2n(n+1)[k_{s_2} a y_n'(k_{s_2} a) - y_n(k_{s_2} a)]$$

$$d_{21} = -k_1 a h_n^{(1)\prime}(k_1)$$

$$d_{22} = k_{d_2} a j_n'(k_{d_2} a)$$

$$d_{23} = k_{d_2} a y_n'(k_{d_2} a)$$

$$d_{24} = n(n+1) j_n(k_{s_2} a)$$

$$d_{25} = n(n+1) y_n(k_{s_2} a)$$

$$d_{32} = 2[j_n(k_{d_2} a) - k_{d_2} a j_n'(k_{d_2} a)]$$

$$d_{33} = 2[y_n(k_{d_2} a) - k_{d_2} a y_n'(k_{d_2} a)]$$

$$d_{34} = 2k_{s_2} a j_n'(k_{s_2} a) + [k_{s_2}^2 a^2 - 2n(n+1) + 2] j_n(k_{s_2} a)$$

$$d_{35} = 2k_{s_2} a y_n'(k_{s_2} a) + [k_{s_2}^2 a^2 - 2n(n+1) + 2] y_n(k_{s_2} a)$$

$$d_{42} = -4k_{d_2} b j_n'(k_{d_2} b) + [2n(n+1) - k_{s_2}^2 b^2] j_n(k_{d_2} b)$$

$$d_{43} = -4k_{d_2} b y_n'(k_{d_2} b) + [2n(n+1) - k_{s_2}^2 a^2] y_n(k_{d_2} b)$$

$$d_{44} = 2n(n+1)[k_{s_2} b j_n'(k_{s_2}) - j_n(k_{s_2} b)]$$

$$d_{45} = 2n(n+1)[k_{d_2} b y_n'(k_{s_2} b) - y_n(k_{s_2} b)]$$

$$d_{46} = \left(\frac{\rho_3}{\rho_2}\right) k_{s_2}^2 b^2 j_n(k_3 b)$$

$$d_{52} = k_{d_2} b j_n'(k_{d_2} b)$$

$$d_{53} = k_{d_2} b y_n'(k_{d_2} b)$$

$$d_{54} = n(n+1)j_n(k_{s_2}b)$$

$$d_{55} = n(n+1)y_n(k_{s_2}b)$$

$$d_{56} = -k_3 b j_n'(k_3 b)$$

$$d_{62} = 2[j_n(k_{d_2}b) - k_{d_2}b j_n'(k_{d_2}b)]$$

$$d_{63} = 2[y_n(k_{d_2}b) - k_{d_2}b y_n'(k_{d_2}b)]$$

$$d_{64} = 2k_{s_2}b j_n'(k_{s_2}b) + [k_{s_2}^2 a^2 - 2n(n+1)+2]j_n(k_{s_2}b)$$

$$d_{65} = 2k_{s_2}b y_n'(k_{s_2}b) + [k_{s_2}^2 a^2 - 2n(n+1)+2]y_n(k_{s_2}b)$$

and also

$$A_1^* = -\left(\frac{\rho_1}{\rho_2}\right)k_{s_2}^2 a^2 j_n(k_1 a)$$

$$A_1^* = k_1 a j_n'(k_1 a).$$